

# Beyond the Noise: Aligning Prompts with Latent Representations in Diffusion Models

Vasco Ramos<sup>1</sup>, Regev Cohen<sup>2</sup>, Idan Szpektor<sup>2</sup>, Joao Magalhaes<sup>1</sup>

NOVA University of Lisbon<sup>1</sup>

Google Research<sup>2</sup>

vcc.ramos@campus.fct.unl.pt

## Abstract

Conditional diffusion models rely on language-to-image alignment methods to steer the generation towards semantically accurate outputs. Despite the success of this architecture, misalignment and hallucinations remain common issues and require automatic misalignment detection tools to improve quality, for example by applying them in a Best-of-N (BoN) post-generation setting. Unfortunately, measuring the alignment after the generation is an expensive step since we need to wait for the overall generation to finish to determine prompt adherence. In contrast, this work hypothesizes that text/image misalignments can be detected early in the denoising process, enabling real-time alignment assessment without waiting for the complete generation. In particular, we propose NoisyCLIP a method that measures semantic alignment in the noisy latent space. This work is the first to explore and benchmark prompt-to-latent misalignment detection during image generation using dual encoders in the reverse diffusion process. We evaluate NoisyCLIP qualitatively and quantitatively and find it reduces computational cost by 50% while achieving 98% of CLIP alignment performance in BoN settings. This approach enables real-time alignment assessment during generation, reducing costs without sacrificing semantic fidelity.<sup>1</sup>

## 1. Introduction

The advances in image generation achieved by diffusion models [2, 16, 35, 41, 42] have opened exciting possibilities for generating realistic images from textual prompts. Reverse diffusion, coupled with cross-attention mechanisms, guides iterative removal of noise, shaping a final image that adheres to the input textual prompt. However, reverse diffusion image generation is a costly process, and there is no inherent guarantee that it will follow the optimal denoising trajectory [1], and it may fail to generate an image that fully

A white cup filled with a latte and topped with a ghost-shaped design, accompanied by a red autumn leaf on a textured surface.

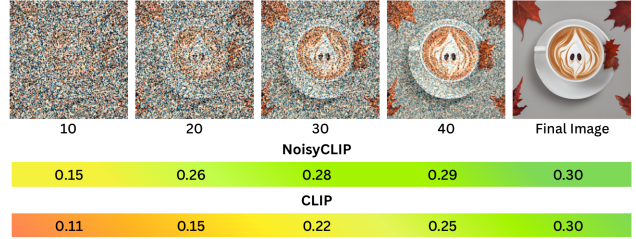


Figure 1. NoisyCLIP measures language-to-latent alignment during reverse diffusion by comparing textual prompts to intermediate latent representations, enabling early detection of misalignments.

adheres to the prompt.

Current methodologies for measuring alignment between textual prompts and images mainly focus on assessing alignment of the output image [14, 23, 26]. Nonetheless, the iterative nature of diffusion models raises a critical question: *is it possible to robustly evaluate alignment during the reverse diffusion process itself, at the intermediate latent representations?* Evaluating solely on the final image results in wasted compute time since misaligned generations must complete the full process before being discarded. This inefficiency is amplified in strategies such as Best-of-N (BoN) selection [24, 28], where the analysis of multiple complete images incurs a substantial collective computational cost. By evaluating alignment at intermediate latent stages, we can implement early stopping for poorly performing denoising processes, thereby saving significant computational resources and improving the efficiency of BoN selection.

Developing metrics for evaluating the intermediate latent steps is non-trivial. Although noise inversion techniques exist [8, 30], there are no open datasets containing intermediate noise sequences, which means implementation differences are inevitable, creating ambiguity and limiting comparative study. To address this critical gap, we introduce the

<sup>1</sup>Code and data will be available for research purposes

first open benchmark for assessing alignment of intermediate latent representations in reverse diffusion processes.

To the best of our knowledge, no prior work has focused specifically on analyzing and understanding methods for inner language-to-latent alignment using twin-tower similarity models (e.g. CLIP). Leveraged by the new dataset, we propose NoisyCLIP, a model designed to improve the comprehension of noisy latent diffusion representations, thereby significantly enhancing the text-image alignment measurement [39], as illustrated in Figure 1. NoisyCLIP allows for the robust identification of misalignments during inference, which enables the early termination of generation or mid-generation BoN sampling. This approach offers considerable computational savings while consistently generating highly aligned images. To summarize, this paper proposes the following contributions:

- We propose NoisyCLIP, a noise-aware model, capable of measuring language-to-latent alignment, even with a high level of noise.
- We introduce two unique datasets for benchmarking language-to-latents alignment: Noisy-Conceptual-Captions and Noisy-GenAI-Bench, each comprising final generated images and their sequence of intermediate latent representations.
- We are the first to apply early stopping of diffusion trajectories in a Best-of-N (BoN) setting, demonstrating that selecting the image at the midpoint of reverse diffusion cuts computational cost by 50%, while achieving 98% performance of the CLIP-based method.

## 2. Related Work

**Text-to-image Generation** models are trained to learn associations between linguistic and visual concepts [53]. Despite previous efforts [13, 22], reverse diffusion models, including DALL-E 2 [38], Imagen [42], and Stable Diffusion [40], have emerged as the predominant approach [2, 10, 33, 35, 40]. Although early diffusion models [16] lacked control over the generation, advances in controllability and quality have been driven by the introduction of textual prompts [20, 40] and further refined through the use of multiple text encoders [35–37].

**Latent Space.** Early diffusion models were constrained by the computationally demanding pixel space [16]. To overcome this inefficiency, newer approaches employ a two-stage process: an autoencoder first maps high-dimensional images into a lower-dimensional latent space, which is then used for the more efficient reverse diffusion process. This strategy significantly reduces computational demands, memory, and training time [40, 43]. Consequently, researchers have increasingly focused on understanding and manipulating this latent space, recognizing that working within it is key to substantially improving the

quality of the output. [6, 32, 39, 51].

We take advantage of this latent space, using the intermediate generations to measure the alignment of the prompt and the image being generated. This allows us to understand the generation’s trajectory and predict the final alignment of the result.

**Alignment Metrics.** Alignment between the generated image and the text input is a key measure to assess the quality of the generative model. Dual encoders such as CLIP [14, 36] and SigLIP [56] provided an early solution by directly measuring the cosine similarity between the image and text representations. More recently, approaches that leverage language models [37] have achieved state-of-the-art results in measuring image-text similarity, demonstrating a high degree of agreement with human judgments [26]. Moreover, utilizing Vision Language Models for evaluation improves generation performance by incorporating models feedback into the process [58]. However, this approach requires a verifier model that may be larger than the generation model, potentially slowing the generation, and has so far only been evaluated on autoregressive models [50], excluding more common diffusion models [40]. To mitigate this, recent work [3] employs a CLIP model to directly receive latent information from the latest diffusion step, bypassing the need to process the full image through the decoder. Additionally, another work [30] presents similar approaches to use latent information to determine the optimal classifier free guidance during the reverse diffusion process.

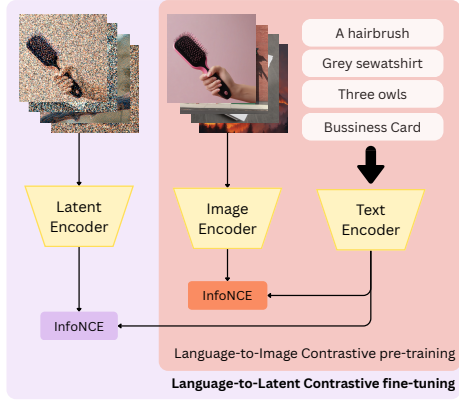
While current metrics successfully assess final image similarity, there’s a critical need for efficient, in-process assessment during reverse diffusion. Existing latent alignment efforts either require full pipeline processing [3] or simply treat alignment as a means to an end [30]. These studies lack a deep, dedicated analysis, open-source models, and standardized comparison data. Our work fills this gap by proposing a novel method and open dataset that leverage intermediate generation data to efficiently assess semantic alignment throughout the diffusion latent space.

## 3. Aligning Language with Noisy Latents

The core challenge of our work is to measure the alignment between the source text and the ambiguous and noisy latent representations generated during reverse diffusion. To address this, we propose a solution based on twin-tower similarity models, such as CLIP, to measure language-to-latent alignment as a similarity problem. This section starts by formalizing the language-to-latent alignment problem (Section 3.1). We then explain how to mitigate the limited availability of noise-corrupted data (Section 3.2), required to train NoisyCLIP as described in Section 3.3. Following this, we propose a new benchmark to evaluate language-to-latent assessment methods (Section 3.4).



### Language-to-Latent Contrastive Training



### Assesment of Language-to-Latent Alignment

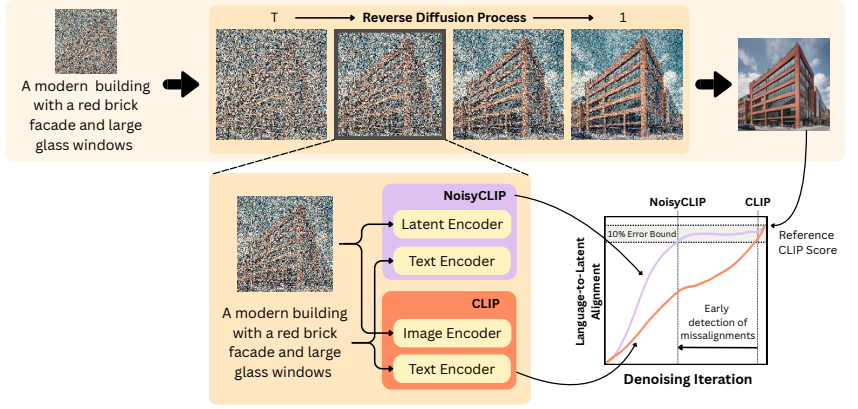


Figure 2. A prompt is used to generate an image, and at an intermediate step, the generated image and the original prompt are encoded and their similarity is measured. As demonstrated, our method generates a similarity score that is closely aligned with the score assessed for the final produced image, while at intermediate stages of generation, allowing for the early identification of misalignments. These results are possible due to the fine-tuning of the image encoder on latent images present on the Noisy-Conceptual-Captions dataset.

### 3.1. Language-to-Latent Alignment Problem

In image generation, earlier techniques such as Classifier-Free Guidance [15] enhance the output quality of diffusion models, but these approaches inherently sacrifice in-process feedback. This limitation leads to the adoption of post-hoc language-image alignment methods, which evaluate the final image after generation, introducing computational inefficiencies and hindering iterative control over the generation process [26, 28]. Despite Latent Diffusion Models [40] grounding generation in textual prompts, there remains no mechanism to leverage this information for real-time feedback during generation. In this section, we explore how to enable direct language-to-latent alignment evaluation during generation, eliminating post-hoc assessment and offering a more scalable and responsive approach to image synthesis. We begin by recalling the objective function of the Latent Diffusion Model:

$$L_{LDM} := \mathbb{E}_{\mathcal{E}(x), y, \epsilon \sim \mathcal{N}(0,1), t} [\|\epsilon - \epsilon_\theta(z_t, t, \tau_\theta(y))\|_2^2] \quad (1)$$

In this formulation,  $x$  is the original image, and  $z = \mathcal{E}(x)$  is its latent representation generated by the encoder  $\mathcal{E}$ .  $z_t$  represents the noisy latent state after  $t$  diffusion steps, where  $t$  ranges from 1 to  $T$ .  $\epsilon$  is the Gaussian noise used to corrupt the latent state, and  $\epsilon_\theta$  is the noise prediction model trained to estimate the noise  $\epsilon$  added to  $z_t$ . The reverse diffusion steps are conditioned by the input text  $y$ , encoded by the text encoder  $\tau_\theta(y)$ . The text embedding  $\tau_\theta(y)$  is then used in cross-attention mechanisms to interact with noisy latent states  $z_t$ , guiding the denoising process towards a text-aligned image. We maintain this standard notation throughout the paper.

To evaluate similarity in the image space, we calculate the cosine similarity between the image and text

prompt [36]. Given the final generated image,  $x$ , and the text prompt,  $y$ , we employ the text encoder,  $\tau_\theta$ , and an image encoder,  $\nu_\theta$ , to compute the similarity score,

$$S_{\text{final}}(x, y) = \tau_\theta(y) \cdot \nu_\theta(x). \quad (2)$$

To generalize this operator to the intermediate diffusion steps, we extend  $S_{\text{final}}(x, y)$  which operates on pixel-space images ( $x$ ), to support latent representations  $z_t$  that cannot be directly inputted into  $\nu_\theta$ . This extension is defined as

$$S_{\text{latent}}(z_t, y) = \tau_\theta(y) \cdot \nu_\theta(\Phi(z_t)), \quad (3)$$

where  $z_t$  is the latent representation at step  $t$ , and  $\Phi$  is the linear transformation (inverse of  $\mathcal{E}$ ) that converts  $z_t$  into an RGB-like space consumable by the image encoder  $\nu_\theta$ , as illustrated in Figure 2. The text prompt  $y$  and the text encoder parameters remain the same as in  $S_{\text{final}}$ .

The definition of  $S_{\text{latent}}$  allows for the assessment of how well image representations align with text prompts during the reverse diffusion process. This approach relies on having access to noise-corrupted data. In the following section, we will explore the scarcity of publicly available data of this kind and explore our approach to generate this kind of data.

### 3.2. Synthesis of Noise-Corrupted Data

**Lack of Latent Data.** There is a notable lack of open data involving noisy latent images. This shortage is often justified by the notion that if noisy images are required, one can simply apply noise inversion techniques to the image without the need to generate or store noisy data [8, 49, 54]. This hinders consistency across different studies and the ability to reproduce previous results and properly compare to them. This highlights the need for an open dataset that comprises noisy latent data.

**Generating Noise from Prompts.** To mitigate the observed lack of open, noisy image data, our training dataset  $\mathcal{D}$  is structured as a collection of samples where each sample within  $\mathcal{D}$  is a tuple of the form  $(y, x, \{z_t\}_{t=1}^T)$ . Where  $y$  represents the image generation prompt,  $x$  is the corresponding generated image and  $\{z_t\}_{t=1}^T$  represents the sequence of latent representations related with the image’s reverse diffusion process.

To optimize the encoder, we use a rewritten version of CC12M [9, 27]. This dataset, which provides shorter and more detailed prompts, ensures caption quality is aligned with the requirements of image generation tasks, building upon the diverse visual concepts present in the original CC12M [5]. Using SDXL [35], we generate images from these prompts and extract latent representations for training (as detailed in Section 4.5). This process captures controlled noise variations in the reverse diffusion process, enabling us to construct high-quality training data for encoder optimization.

### 3.3. Language-to-Latent Contrastive Training

To improve noise robustness in pre-trained vision encoders, we introduce NoisyCLIP, a twin-tower encoder capable of measuring similarity earlier in the reverse diffusion process.

We select a fixed latent interval (20–29) for contrastive training to enable stable language-to-latent alignment across diverse representations using only a subset of the data, as validated in Section 5.4.1. Using the generated noisy latents  $z_t$ , we exclusively fine-tune the image encoder (see Figure 2). During the contrastive learning, each noisy latent representation  $z_t$  forms a positive pair with its corresponding text prompt  $y$ , while being contrasted against in-batch negatives  $\mathcal{N}$  (all image-text pairs in the batch except the positive pair).

By applying the contrastive loss (InfoNCE) [46] we maximize similarity between positive pairs  $(z_t, y)$  while suppressing similarity with negatives  $\mathcal{N}$ . Freezing the text encoder maintains its general-purpose functionality while optimizing language-to-latent alignment through image encoder tuning. The crucial advantage of this approach is that the frozen text encoder can be shared with the diffusion model, which ensures consistency between textual representations and the diffusion model’s conditioning space. This grounding forces the latent encoder to align better with the diffusion representations, effectively mimicking the cross-attention interaction during denoising while providing an early projection of final image alignment [20].

### 3.4. Benchmark Proposal

Lastly, to overcome the lack of standardized data to evaluate representations in inner diffusion processes, we propose a benchmark built on top of image captioning [5] and image generation [24] datasets. We derive two sub-

sets, Noisy-Conceptual-Captions and Noisy-GenAI-Bench to enable open, systematic community evaluation across three critical dimensions.

**Diverse visual representations.** To evaluate inner diffusion representations, we generate multiple images for each prompt  $p$ , allowing us to quantify how alignment metrics choose the output that most closely matches the prompt across diverse visual representations.

**Factual consistency.** We employ a classification task where a single image is evaluated against  $k$  prompts, one correct and  $k - 1$  intentionally corrupted to systematically violate factual consistency (as detailed in the Appendix). This approach improves the robustness of the evaluation compared to random prompt sampling by introducing targeted factual violations rather than random information.

**Noisy Latent Information.** To support the assessment of the previously described tasks in the reverse diffusion process, we store the noisy latent information at each denoising step during generation.

## 4. Experimental Setup

In this section, we provide a detailed description of our evaluation settings, including tasks, datasets, baseline models, metrics, and implementation details.

### 4.1. Evaluation Tasks

To evaluate the proposed method, we conducted the following experiments:

- **Language-to-Latent Alignment.** We start by examining the language-to-latent alignment throughout the denoising process of  $N$  competing random seeds. We measure the alignment with NoisyCLIP and CLIP, and compare the difference between the best and the worst images (VQAScore is used to rank images by their alignment with the prompt). This allows us to observe how early NoisyCLIP can detect misalignments.
- **Best-of-N:** Our main experiment follows recent work [26, 28] that demonstrated a significant improvement in image quality by generating multiple images and selecting the most aligned one. In our setting, instead of completing all denoising processes, we leverage NoisyCLIP early misalignment detection capabilities, and evaluate how early it can stop poorly aligned denoising processes and keep the best language-to-latent aligned one.
- **Factual Consistency:** As an additional experiment, we assess the model’s ability to assign the highest score to the most factually accurate prompt. This experiment aims to analyze NoisyCLIP in the presence of captions that include non-factual distractors. This evaluation is crucial

as it tests the model’s capacity to distinguish the correct caption from highly similar, yet non-factual, errors. Ultimately, success on this task suggests that the model possesses the semantic understanding required to prevent non-factual image selections during generation.

## 4.2. Datasets

For the experiments explained above, we use two datasets. Specifically, the test sets are:

- **Noisy-Conceptual-Captions**[5]: This subset from our benchmark comprises a set of 1000 captions sampled to enable objective assessment of factual caption selection. This dataset comprises the original prompts, four generated images per original prompt as well as four non-factual prompts ( the creation of these prompts is detailed in the Appendix).
- **Noisy-GenAI-Bench** [24]: This dataset includes a total of 1,600 prompts, consisting of 730 basic prompts and 870 more advanced ones, going from simple compositions such as objects (e.g. "a dog") to more complex compositions such as counting or negations. To evaluate the performance on the BoN task, we expand this dataset by generating 10 images along with the corresponding latent information for each prompt.

## 4.3. Baselines

Our primary method (NoisyCLIP) relies on CLIP [36], with SigLIP [56] used for comparative analysis. Both architectures are evaluated using their pre-trained versions, which serve as the baselines for assessing our methodology. We utilize the base versions for ablation studies and the large versions for presenting the main results. All images were generated using Stable Diffusion XL [35].

## 4.4. Evaluation Metrics

For the BoN task, we assess the model’s ability to select the most relevant image for a given prompt. VQA-based evaluation methods have shown improved reliability and alignment with human assessments [7, 17, 18, 24, 55]. Similarly to previous research, we adopt VQAScore [26] as our primary metric to measure how well encoders can select the most similar image over others for a certain prompt [2, 4, 12, 28, 45, 48].

In the Image-Alignment task, we presented each image with a single correct prompt and multiple non-factual prompts, measuring performance using Recall@1 (R@1) [11, 34, 57, 59]. This metric quantifies the model’s accuracy by measuring the proportion of images in which the correct prompt is ranked first among all candidates.

## 4.5. Implementation Details

**Training.** We fine-tune solely the visual encoder of the dual-encoder on a dataset of 50,000 latents, which are uni-

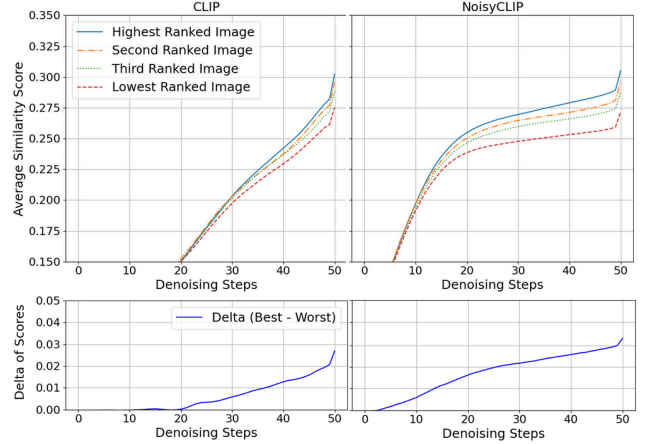


Figure 3. Analysis of alignment measurement throughout the reverse diffusion process shows that our model distinctly separates aligned from misaligned images as soon as latent 20.

formly sampled from the generated images. Training is done with a learning rate of  $5.7e-5$ , using a cosine annealing scheduler with a warm-up ratio of 0.1 and a weight decay of 0.1. All computations are performed on an NVIDIA A100 40G GPU over 10 epochs with a batch size of 128.

**Latent RGB Representation.** Although SDXL [40] latent space utilizes a four-channel structure, direct visualization requires transforming these latents into RGB space. This transformation is done by decoding latent representations via a linear transformation to RGB [47].

## 5. Results and Discussions

This section quantifies our method’s benefits for language-to-latent alignment. We analyze the Best-of-N (BoN) Diffusion strategy (with qualitative results) and assess NoisyCLIP’s factual consistency detection using non-factual prompts. We conclude by exploring the impact of latent ranges and backbone architectures. Ablation studies are in the Appendix.

### 5.1. Measuring Language-to-Latent Alignment

We evaluate language-to-latent alignment effectiveness on a setting of one prompt and four ranked images, computing the VQAScore for each image-prompt pair to establish a reference ranking. Based on this ranking, we calculate the similarity scores for both NoisyCLIP and CLIP for each of these pairs, reporting the average score each model assigns to images in that established rank. For this experiment we use the prompts from the Noisy-Conceptual-Captions dataset as well as the four generated images.

As illustrated in Figure 3, our model effectively discriminates the top image from sub-optimal ones as early as latent

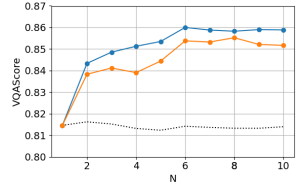
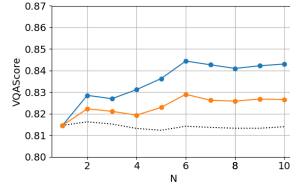
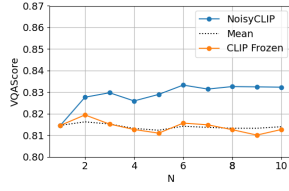
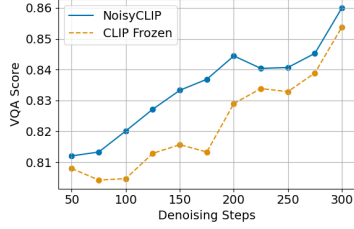


Figure 4. Alignment (VQAScore) vs Figure 5. Best-of-N results for latents 20 and 30 as well as in the final image. The plots compare Best-of-N denoising cost. Cost is normalized for a scenario where  $N = 6$ . NoisyCLIP (blue line) with CLIP (orange line) in a BoN setting. The alignment of the selected image with the prompt is assessed using the VQAScore.

20. It reliably maintains a separation between the images during the reverse diffusion process, achieving a gap above 3%. We can see that our method increases the delta between the highest and lowest scoring images since the initial latents surpass 2% in the middle of the generation. Although our approach focuses on the noisy images, the results do not show any deterioration in the image dimensions. Rather, they show an enhancement that aligns with the trend of the latent dimension, as shown by the leap at the end of each plot (Figure 3).

In contrast, CLIP exhibited persistent difficulty maintaining a separation between the highest and lowest scoring images. Although it can achieve a delta of around 2.5% in the image dimension, most of the generation remains under 1% (up to the mid-30s), with this delta appearing only after latent 20. The transition to the image dimension also resulted in a noticeable shift in scores.

This results shows that our approach makes it feasible to measure the similarity in intermediate latent areas, while maintaining a final score comparable to those obtained with the frozen CLIP. Furthermore, it illustrates the possibility of producing scores that increase nearly linearly from the start of the generation, whereas CLIP only accomplishes this from the midpoint to the conclusion of the generation.

## 5.2. Improving Generation via Best-of-N

To further evaluate our fine-tuning approach with noisy latent information, we analyze NoisyCLIP performance as a ranker on a BoN denoising task. We evaluate model’s ability to select a candidate image by denoising multiple seeds with the same prompt, and scoring the latents according to its alignment with the prompt. This enables the early stopping of denoising processes that are estimated to be sub-optimal, thus reducing the aggregated number of denoising iterations. This experiment aims to determine how our model improves the BoN performance on the GenAI-Bench basic prompts. A detailed analysis of the performance on the basic and advanced prompts is provided in the Appendix.

**Defining Denoising Iterations as a Metric for Cost.** The following experiment investigate how assessing this alignment in mid-reverse diffusion affects the total computational cost when generating multiple images simultaneously. We define cost by the number of reverse diffusion steps required to produce an image; in our baseline [35], this is 50 steps per image. If BoN is applied at a certain stage, only one image proceeds with the generation. For example, if two images begin generation but only one is selected to continue at latent stage 25, the total cost becomes  $(25 \times 2) + (25 \times 1) = 75$ , representing a 25% saving compared to a full ”best-of-2” approach ( $2 \times 50 = 100$ ).

**Performance Gains Versus Costs Reduction.** In Figure 4 we analyze the trade-off between prompt alignment (VQAScore) and computational cost within a specific best-of-N selection scenario ( $N = 6$  in this setting). The standard baseline, which uses CLIP to select the final image after all 6 generations are complete, achieves a VQAScore of 0.85 at a cost of 300 ( $= 6 \times 50$ ).

By using 150 denoising steps, we cut the denoising iterations by 50% (Cost 150), accepting only a minimal 2% reduction in VQAScore compared to the full baseline. Notably, at this reduced cost, the traditional CLIP approach performs 2% worse than our method. Furthermore, at a cost of 200 (a one-third reduction in computation), our method achieves the highest latent image selection score. Altogether, across the entire reverse diffusion process, our approach consistently outperforms the baseline, demonstrating a superior balance between alignment and efficiency.

**Selecting images in the latent space.** In this analysis, Figure 5, we compare the performance of our method on Best-of-N denoising task, with  $N = \{1, \dots, 10\}$ . When applying a dual encoder to rank the N generations in latent 20 (Figure 5a), the baseline’s results are similar to the average alignment of all images generated in all N approaches, showing that applying the CLIP model in this case does not bring any benefit in terms of alignment. On the other hand, our method improves alignment by about 1%, maintaining these gains across all tested n’s, showing our approach ef-














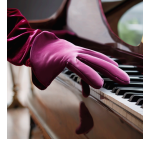






	A cream colored labradoodle is on the right of a black cat with white ears.	An oil painting of a majestic lion hanging above the fireplace.	The soft, woolen blanket draped over a plush, velvet couch.	A tall cactus in a terracotta pot next to a short succulent in a ceramic bowl.	A cat wearing a tiny hat sits under a table.	Velvet gloves resting on the polished, wooden surface of a piano.	Cost (diffusion steps)
CLIP							300
CLIP							150
NoisyCLIP							150

Figure 6. Images are generated using a best-of-6 strategy. Our proposed method is compared against the standard CLIP baseline at two computation budgets: a fixed, lower cost of 150 diffusion steps and the full cost of 300 diffusion steps (generating all 6 images). Our approach demonstrates superior image alignment compared to the standard method at the fixed 150-step budget. Furthermore, NoisyCLIP achieves comparable, or even higher, alignment than the full 300-step baseline while using half of the steps.

fectiveness dealing with noisy images improving even over the CLIP selection in latent 30 (Figure 5b).

Figure 5c shows results for the compute-intensive final image selection, where all images are fully generated. Although the baseline benefits from the low noise (since CLIP wasn’t trained on noisy images), our method consistently achieves superior prompt alignment across all selections. Specifically, the baseline reaches a 0.84 VQAScore with best-of-4 selection at a cost of 200 (Figure 5c). Our method surpasses this score using a best-of-6 selection at latent step 30 (Figure 5b) at the same computational cost. Notably, to match our resulting best-of-6 VQAScore, the baseline requires at least 20% more computation.

**Qualitative Results.** Figure 6 demonstrates that our method achieves high-fidelity image selection in a best-of-6 setting using only 150 diffusion steps, while consistently matching or surpassing CLIP selection performance as seen in the first and second prompt. For simple prompts (e.g. the third prompt), all approaches select text-aligned images, confirming that generation models can mostly fulfill low-complexity queries. Critically, this contrasts with complex prompts like *“a tall cactus in a terracotta pot next to a short succulent in a ceramic bowl”* (fourth prompt), where only our method correctly maintains all three attributes: cactus height, pot material, and succulent bowl type. CLIP with half of the cost hallucinates two cacti, while using the total of diffusion steps misrepresents cactus height. Similarly, for the fifth and sixth prompts, NoisyCLIP resolves subtle spatial relationships such as selecting a cat under a table

and distinguishing resting gloves from gloves on a piano-playing hand (where CLIP with the same cost fails).

These results validate our hypothesis that early detection of misalignment enables alignment improvement without requiring full image generation. A detailed analysis of failure cases and edge scenarios is provided in the Appendix.

### 5.3. Factual Consistency

This experiment assesses the ability of NoisyCLIP and the baseline model to select the correct caption for a given image from a set of 5 candidates (1 correct, 4 non-factual). Figure 7 presents the recall@1 for each model, with results that NoisyCLIP discriminates the best from the worst caption remarkably early, at latent 10, while CLIP requires an extra 20 denoise iterations to the same result (as shown by the shadowed regions in Figure 7).

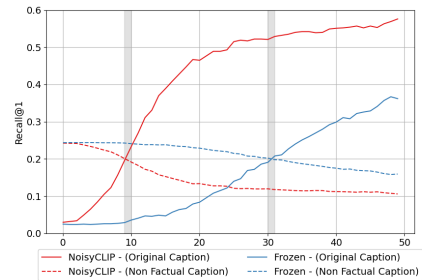


Figure 7. Recall@1 for Caption Selection. The solid line shows the score for the original ground-truth caption, and the dashed line shows the average score of the non-factual distractors.

Despite NoisyCLIP’s significant performance gains, the trend that emerges across denoising iterations is that both models increasingly select the correct caption over non-factual ones. Within the first 25 iterations, NoisyCLIP recall for the correct caption increases from near 0 to surpass the 0.5 mark, whereas the baseline just rises below 0.1. It is also worth noting that NoisyCLIP recall tends to stabilize in the second half of the generation, while the baseline method ends up never exceeding 0.4. We provide an analysis on the multiple non-factual caption selection in the Appendix.

## 5.4. Further Analysis

### 5.4.1. Impact of Training Latent Ranges on Inference

In this experiment we examine how different training latent ranges impact NoisyCLIP performance. Results are reported on the Noisy-Concept-Captions dataset. As shown in Figure 8, the alignment performance correlate with the inference latent range: lower latent ranges result in less accurate alignment, underscoring the challenge of assessing language-to-latent alignment under the presence of noise.

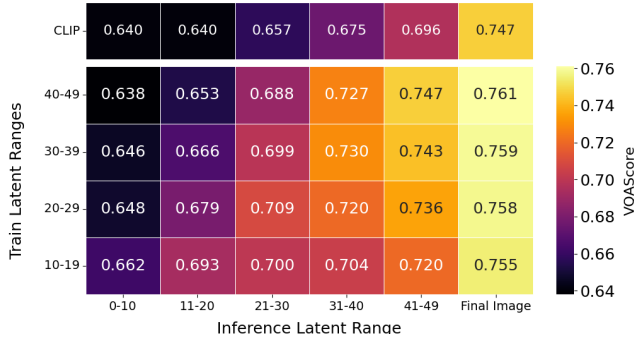


Figure 8. Performance across inference ranges (columns) when trained with different latent ranges (rows). The analysis highlights the correlation the different latent distributions.

The baseline CLIP model (top row), performs poorly in latents ranges 1-49 achieving a top performance of 0.696, despite a VQAScore of 0.747 on the final image. This disparity highlights the limitation of lacking noisy data training. By comparison, our approach shows that NoisyCLIP inference performance generally correlates with the level of noise present during training. Low-noise training (ranges 40-49) consistently yields the best overall results in both the final latent range and the final image. However, models trained on initial latent ranges (10-19) perform best early on (up to 4 points gain) but decline sharply in the final two ranges. Middle-range training (20-29) strikes the best balance, achieving stable performance: it is comparable to the best (40-49) models in the later inference ranges while performing better in the initial ranges. These results indicate that moderate training noise (latent ranges 20–29) optimizes balanced performance across inference stages.

Table 1. Performance comparison in latent and image spaces. We report Factual Consistency (R@1) and Best-of-N (VQAScore).

Model	Fact. Consist. (R@1)	Best-of-N (VQAScore)
<i>Denoised Latent (iteration 21-30)</i>		
NoisyCLIP	<b>0.506</b>	<u>0.709</u>
CLIP L14	0.145	0.657
NoisySigLIP	<u>0.194</u>	<b>0.718</b>
SigLIP L16	0.147	0.652
<i>Final Image (iteration 50)</i>		
CLIP L14	–	0.747
SigLIP L16	–	0.764

### 5.4.2. Backbone models

Lastly, Table 1 demonstrates that our approach enhances each model performance over its baseline. For instance, in the latent alignment task (R@1), our method (NoisyCLIP) increases CLIP performance by up to 3.5 times and achieves a VQAScore of 0.709, exceeding the baseline by over 5%. In the Best-of-N task, it reaches 95% of the final baseline performance midway through reverse diffusion, highlighting robustness even with significant noise.

When applied to an alternative backbone, SigLIP, our approach (NoisySigLIP) yields Best-of-N performance comparable to NoisyCLIP. Crucially, this improvement does not generalize to latent alignment, where NoisySigLIP lags NoisyCLIP by a factor of 2.6 in R@1, indicating that the specific gains observed with CLIP are not immediately transferable across different contrastive backbones.

## 6. Conclusions

In this work, we introduced NoisyCLIP, a framework for evaluating language-to-latent alignment during the reverse diffusion process by quantifying similarity across intermediate latent representations. Empirical evaluations demonstrate that NoisyCLIP provides substantial advantages in Best-of-N generation strategies by enabling early-stage discrimination of higher-quality samples. This capability leads to more efficient use of computational resources, reducing the number of required diffusion iterations by up to 50% while preserving the fidelity of the final outputs relative to a full cost solution.

Collectively, these findings establish the feasibility of continuous, in-process alignment evaluation within latent diffusion models. By leveraging iterative latent information, NoisyCLIP transforms alignment assessment from a purely post-hoc procedure into an integral component of the generation process advancing the development of adaptive, controllable, and computationally efficient multimodal generative systems.

## References

- [1] Aishwarya Agarwal, Srikrishna Karanam, K. J. Joseph, Apoorv Saxena, Koustava Goswami, and Balaji Vasan Srinivasan. A-STAR: test-time attention segregation and retention for text-to-image synthesis. In *IEEE/CVF International Conference on Computer Vision, ICCV 2023, Paris, France, October 1-6, 2023*, pages 2283–2293. IEEE, 2023. 1
- [2] Jason Baldridge, Jakob Bauer, Mukul Bhutani, Nicole Brich-tova, Andrew Bunner, Kelvin Chan, Yichang Chen, Sander Dieleman, Yuqing Du, Zach Eaton-Rosen, Hongliang Fei, Nando de Freitas, Yilin Gao, Evgeny Gladchenko, Sergio Gómez Colmenarejo, Mandy Guo, Alex Haig, Will Hawkins, Hexiang Hu, Huilian Huang, Tobenna Peter Igwe, Christos Kaplanis, Siavash Khodadadeh, Yelin Kim, Ksenia Konyushkova, Karol Langner, Eric Lau, Shixin Luo, Sona Mokrá, Henna Nandwani, Yasumasa Onoe, Aaron van den Oord, Zarana Parekh, Jordi Pont-Tuset, Hang Qi, Rui Qian, Deepak Ramachandran, Poorva Rane, Abdullah Rashwan, Ali Razavi, Robert Riachi, Hansa Srinivasan, Srivatsan Srinivasan, Robin Strudel, Benigno Uria, Oliver Wang, Su Wang, Austin Waters, Chris Wolff, Auriel Wright, Zhisheng Xiao, Hao Xiong, Keyang Xu, Marc van Zee, Junlin Zhang, Katie Zhang, Wenlei Zhou, Konrad Zolna, Ola Aboubakar, Canfer Akbulut, Oscar Akerlund, Isabela Albuquerque, Nina Anderson, Marco Andreetto, Lora Aroyo, Ben Bariach, David Barker, Sherry Ben, Dana Berman, Courtney Biles, Irina Blok, Pankil Botadra, Jenny Brennan, Karla Brown, John Buckley, Rudy Bunel, Elie Bursztin, Christina Butterfield, Ben Caine, Viral Carpenter, Norman Casagrande, Ming-Wei Chang, Solomon Chang, Shamik Chaudhuri, Tony Chen, John Choi, Dmitry Churbanau, Nathan Clement, Matan Cohen, Forrester Cole, Mikhail Dektiarev, Vincent Du, Pra-neet Dutta, Tom Eccles, Ndidi Elue, Ashley Feden, Shlomi Fruchter, Frankie Garcia, and Roopal Garg. Imagen 3. *CoRR*, abs/2408.07009, 2024. 1, 2, 5
- [3] Jason Becker, Chris Wendler, Peter Baylies, Robert West, and Christian Wressnegger. Controlling latent diffusion using latent CLIP. *CoRR*, abs/2503.08455, 2025. 2
- [4] Paola Cascante-Bonilla, Yu Hou, Yang Trista Cao, Hal Daumé III, and Rachel Rudinger. Natural language inference improves compositionality in vision-language models. In *The Thirteenth International Conference on Learning Representations, ICLR 2025, Singapore, April 24-28, 2025*. OpenReview.net, 2025. 5
- [5] Soravit Changpinyo, Piyush Sharma, Nan Ding, and Radu Soricut. Conceptual 12m: Pushing web-scale image-text pre-training to recognize long-tail visual concepts. In *IEEE Conference on Computer Vision and Pattern Recognition, CVPR 2021, virtual, June 19-25, 2021*, pages 3558–3568. Computer Vision Foundation / IEEE, 2021. 4, 5
- [6] Hila Chefer, Oran Lang, Mor Geva, Volodymyr Polosukhin, Assaf Shocher, Michal Irani, Inbar Mosseri, and Lior Wolf. The hidden language of diffusion models. In *The Twelfth International Conference on Learning Representations, ICLR 2024, Vienna, Austria, May 7-11, 2024*. OpenReview.net, 2024. 2
- [7] Jaemin Cho, Abhay Zala, and Mohit Bansal. Visual programming for step-by-step text-to-image generation and evaluation. In *Advances in Neural Information Processing Systems 36: Annual Conference on Neural Information Processing Systems 2023, NeurIPS 2023, New Orleans, LA, USA, December 10 - 16, 2023*, 2023. 5
- [8] Wenkai Dong, Song Xue, Xiaoyue Duan, and Shumin Han. Prompt tuning inversion for text-driven image editing using diffusion models. In *IEEE/CVF International Conference on Computer Vision, ICCV 2023, Paris, France, October 1-6, 2023*, pages 7396–7406. IEEE, 2023. 1, 3
- [9] Caption Emporium. conceptual-captions-cc12m-llavanext. <https://huggingface.co/datasets/CaptionEmporium/conceptual-captions-cc12m-llavanext>, 2024. 4
- [10] Patrick Esser, Sumith Kulal, Andreas Blattmann, Rahim Entezari, Jonas Müller, Harry Saini, Yam Levi, Dominik Lorenz, Axel Sauer, Frederic Boesel, Dustin Podell, Tim Dockhorn, Zion English, and Robin Rombach. Scaling rectified flow transformers for high-resolution image synthesis. In *Forty-first International Conference on Machine Learning, ICML 2024, Vienna, Austria, July 21-27, 2024*. OpenReview.net, 2024. 2
- [11] Keren Ganon, Morris Alper, Rachel Mikulinsky, and Hadar Averbuch-Elor. WAFFLE: multimodal floorplan understanding in the wild. In *IEEE/CVF Winter Conference on Applications of Computer Vision, WACV 2025, Tucson, AZ, USA, February 26 - March 6, 2025*, pages 1488–1497. IEEE, 2025. 5
- [12] Leander Gierbach, Stephan Alaniz, Genevieve Smith, and Zeynep Akata. A large scale analysis of gender biases in text-to-image generative models. *CoRR*, abs/2503.23398, 2025. 5
- [13] Ian J. Goodfellow, Jean Pouget-Abadie, Mehdi Mirza, Bing Xu, David Warde-Farley, Sherjil Ozair, Aaron Courville, and Yoshua Bengio. Generative adversarial nets. In *Advances in Neural Information Processing Systems*. Curran Associates, Inc., 2014. 2
- [14] Jack Hessel, Ari Holtzman, Maxwell Forbes, Ronan Le Bras, and Yejin Choi. Clipscore: A reference-free evaluation metric for image captioning. In *Proceedings of the 2021 Conference on Empirical Methods in Natural Language Processing, EMNLP 2021, Virtual Event / Punta Cana, Dominican Republic, 7-11 November, 2021*, pages 7514–7528. Association for Computational Linguistics, 2021. 1, 2
- [15] Jonathan Ho and Tim Salimans. Classifier-free diffusion guidance. In *NeurIPS 2021 Workshop on Deep Generative Models and Downstream Applications*, 2021. 3
- [16] Jonathan Ho, Ajay Jain, and Pieter Abbeel. Denoising Diffusion Probabilistic Models. In *Advances in Neural Information Processing Systems*, pages 6840–6851. Curran Associates, Inc., 2020. 1, 2
- [17] Yushi Hu, Benlin Liu, Jungo Kasai, Yizhong Wang, Mari Ostendorf, Ranjay Krishna, and Noah A. Smith. TIFA: accurate and interpretable text-to-image faithfulness evaluation with question answering. In *IEEE/CVF International Conference on Computer Vision, ICCV 2023, Paris, France, October 1-6, 2023*, pages 20349–20360. IEEE, 2023. 5



- [18] Kaiyi Huang, Kaiyue Sun, Enze Xie, Zhenguo Li, and Xihui Liu. T2i-compbench: A comprehensive benchmark for open-world compositional text-to-image generation. In *Advances in Neural Information Processing Systems 36: Annual Conference on Neural Information Processing Systems 2023, NeurIPS 2023, New Orleans, LA, USA, December 10 - 16, 2023*, 2023. 5
- [19] Wen Huang, Hongbin Liu, Minxin Guo, and Neil Gong. Visual hallucinations of multi-modal large language models. In *Findings of the Association for Computational Linguistics: ACL 2024*, pages 9614–9631, Bangkok, Thailand, 2024. Association for Computational Linguistics. 13
- [20] Andrew Jaegle, Felix Gimeno, Andy Brock, Oriol Vinyals, Andrew Zisserman, and João Carreira. Perceiver: General perception with iterative attention. In *Proceedings of the 38th International Conference on Machine Learning, ICML 2021, 18-24 July 2021, Virtual Event*, pages 4651–4664. PMLR, 2021. 2, 4
- [21] Aishwarya Kamath, Johan Ferret, Shreya Pathak, Nino Vieillard, Ramona Merhej, Sarah Perrin, Tatiana Matejovicova, Alexandre Ramé, Morgane Rivi  re, Louis Rouillard, Thomas Mesnard, Geoffrey Cideron, Jean-Bastien Grill, Sabela Ramos, Edouard Yvinec, Michelle Casbon, Etienne Pot, Ivo Penchev, Ga  l Liu, Francesco Visin, Kathleen Kenealy, Lucas Beyer, Xiaohai Zhai, Anton Tsitsulin, R  bert Busa-Fekete, Alex Feng, Naveen Sachdeva, Benjamin Coleman, Yi Gao, Basil Mustafa, Iain Barr, Emilio Parisotto, David Tian, Matan Eyal, Colin Cherry, Jan-Thorsten Peter, Danila Sinopalnikov, Surya Bhupatiraju, Rishabh Agarwal, Mehran Kazemi, Dan Malkin, Ravin Kumar, David Vilar, Idan Brusilovsky, Jiaming Luo, Andreas Steiner, Abe Friesen, Abhanshu Sharma, Abheesh Sharma, Adi Mayrav Gilady, Adrian Goedeckemeyer, Alaa Saade, Alexander Kolesnikov, Alexei Bendebury, Alvin Abdagic, Amit Vadi, Andr  s Gy  rgy, Andr   Susano Pinto, Anil Das, Ankur Bapna, Antoine Miech, Antoine Yang, Antonia Paterson, Ashish Shenoy, Ayan Chakrabarti, Bilal Piot, Bo Wu, Bobak Shahriari, Bryce Petrini, Charlie Chen, Charline Le Lan, Christopher A. Choquette-Choo, CJ Carey, Cormac Brick, Daniel Deutsch, Danielle Eisenbud, Dee Cattle, Derek Cheng, Dimitris Paparas, Divyashree Shivakumar Sreepathihalli, Doug Reid, Dustin Tran, Dustin Zelle, Eric Noland, Erwin Huizenga, Eugene Kharitonov, Frederick Liu, Gagik Amirkhanyan, Glenn Cameron, Hadi Hashemi, Hanna Klimczak-Plucinska, Harman Singh, Harsh Mehta, Harshal Tushar Lehri, Hussein Hazimeh, Ian Ballantyne, Idan Szpektor, and Ivan Nardini. Gemma 3 technical report. *CoRR*, abs/2503.19786, 2025. 13
- [22] Diederik P Kingma and Max Welling. Auto-encoding variational bayes, 2022. 2
- [23] Yuval Kirstain, Adam Polyak, Uriel Singer, Shahbuland Matiana, Joe Penna, and Omer Levy. Pick-a-pic: An open dataset of user preferences for text-to-image generation. In *Advances in Neural Information Processing Systems 36: Annual Conference on Neural Information Processing Systems 2023, NeurIPS 2023, New Orleans, LA, USA, December 10 - 16, 2023*, 2023. 1
- [24] Baiqi Li, Zhiqiu Lin, Deepak Pathak, Jiayao Li, Yixin Fei, Kewen Wu, Tiffany Ling, Xide Xia, Pengchuan Zhang, Graham Neubig, and Deva Ramanan. Genai-bench: Evaluating and improving compositional text-to-visual generation. *CoRR*, abs/2406.13743, 2024. 1, 4, 5, 14
- [25] Dingkan Liang, Jiahao Xie, Zhikang Zou, Xiaoqing Ye, Wei Xu, and Xiang Bai. Crowdclip: Unsupervised crowd counting via vision-language model. In *IEEE/CVF Conference on Computer Vision and Pattern Recognition, CVPR 2023, Vancouver, BC, Canada, June 17-24, 2023*, pages 2893–2903. IEEE, 2023. 13
- [26] Zhiqiu Lin, Deepak Pathak, Baiqi Li, Jiayao Li, Xide Xia, Graham Neubig, Pengchuan Zhang, and Deva Ramanan. Evaluating text-to-visual generation with image-to-text generation. In *Computer Vision - ECCV 2024 - 18th European Conference, Milan, Italy, September 29-October 4, 2024, Proceedings, Part IX*, pages 366–384. Springer, 2024. 1, 2, 3, 4, 5, 14
- [27] Haotian Liu, Chunyuan Li, Yuheng Li, Bo Li, Yuanhan Zhang, Sheng Shen, and Yong Jae Lee. Llava-next: Improved reasoning, ocr, and world knowledge, 2024. 4
- [28] Nanye Ma, Shangyuan Tong, Haolin Jia, Hexiang Hu, Yu-Chuan Su, Mingda Zhang, Xuan Yang, Yandong Li, Tommi S. Jaakkola, Xuhui Jia, and Saining Xie. Scaling inference time compute for diffusion models. In *IEEE/CVF Conference on Computer Vision and Pattern Recognition, CVPR 2025, Nashville, TN, USA, June 11-15, 2025*, pages 2523–2534. Computer Vision Foundation / IEEE, 2025. 1, 3, 4, 5
- [29] Roni Paiss, Ariel Ephrat, Omer Tov, Shiran Zada, Inbar Mosseri, Michal Irani, and Tali Dekel. Teaching CLIP to count to ten. In *IEEE/CVF International Conference on Computer Vision, ICCV 2023, Paris, France, October 1-6, 2023*, pages 3147–3157. IEEE, 2023. 13
- [30] Pinelopi Papalampidi, Olivia Wiles, Ira Ktena, Aleksandar Shtedritski, Emanuele Bugliarello, Ivana Kajic, Isabela Albuquerque, and Aida Nematzadeh. Dynamic classifier-free diffusion guidance via online feedback. *CoRR*, abs/2509.16131, 2025. 1, 2
- [31] Junsung Park, Jungbeom Lee, Jongyoon Song, Sangwon Yu, Dahuin Jung, and Sungroh Yoon. Know “no” better: A data-driven approach for enhancing negation awareness in clip. In *Proceedings of the IEEE/CVF International Conference on Computer Vision (ICCV)*, pages 2825–2835, 2025. 15
- [32] Yong-Hyun Park, Mingi Kwon, Jaewoong Choi, Junghyo Jo, and Youngjung Uh. Understanding the latent space of diffusion models through the lens of riemannian geometry. In *Advances in Neural Information Processing Systems 36: Annual Conference on Neural Information Processing Systems 2023, NeurIPS 2023, New Orleans, LA, USA, December 10 - 16, 2023*, 2023. 2
- [33] William Peebles and Saining Xie. Scalable diffusion models with transformers. In *IEEE/CVF International Conference on Computer Vision, ICCV 2023, Paris, France, October 1-6, 2023*, pages 4172–4182. IEEE, 2023. 2
- [34] Gensheng Pei, Tao Chen, Yujia Wang, Xinhao Cai, Xiangbo Shu, Tianfei Zhou, and Yazhou Yao. Seeing what matters: Empowering CLIP with patch generation-to-selection.



- In *IEEE/CVF Conference on Computer Vision and Pattern Recognition, CVPR 2025, Nashville, TN, USA, June 11-15, 2025*, pages 24862–24872. Computer Vision Foundation / IEEE, 2025. 5
- [35] Dustin Podell, Zion English, Kyle Lacey, Andreas Blattmann, Tim Dockhorn, Jonas Müller, Joe Penna, and Robin Rombach. SDXL: Improving Latent Diffusion Models for High-Resolution Image Synthesis. In *The Twelfth International Conference on Learning Representations, ICLR 2024, Vienna, Austria, May 7-11, 2024*. OpenReview.net, 2024. 1, 2, 4, 5, 6
- [36] Alec Radford, Jong Wook Kim, Chris Hallacy, Aditya Ramesh, Gabriel Goh, Sandhini Agarwal, Girish Sastry, Amanda Askell, Pamela Mishkin, Jack Clark, Gretchen Krueger, and Ilya Sutskever. Learning transferable visual models from natural language supervision. In *Proceedings of the 38th International Conference on Machine Learning, ICML 2021, 18-24 July 2021, Virtual Event*, pages 8748–8763. PMLR, 2021. 2, 3, 5
- [37] Colin Raffel, Noam Shazeer, Adam Roberts, Katherine Lee, Sharan Narang, Michael Matena, Yanqi Zhou, Wei Li, and Peter J. Liu. Exploring the limits of transfer learning with a unified text-to-text transformer. *J. Mach. Learn. Res.*, 21: 140:1–140:67, 2020. 2
- [38] Aditya Ramesh, Prafulla Dhariwal, Alex Nichol, Casey Chu, and Mark Chen. Hierarchical text-conditional image generation with clip latents. *arXiv preprint arXiv:2204.06125*, 1 (2):3, 2022. 2
- [39] Vasco Ramos, Yonatan Bitton, Michal Yarom, Idan Szpektor, and Joao Magalhaes. Contrastive sequential-diffusion learning: Non-linear and multi-scene instructional video synthesis. In *2025 IEEE/CVF Winter Conference on Applications of Computer Vision (WACV)*, pages 4645–4654, 2025. 2
- [40] Robin Rombach, Andreas Blattmann, Dominik Lorenz, Patrick Esser, and Björn Ommer. High-resolution image synthesis with latent diffusion models. In *IEEE/CVF Conference on Computer Vision and Pattern Recognition, CVPR 2022, New Orleans, LA, USA, June 18-24, 2022*, pages 10674–10685. IEEE, 2022. 2, 3, 5
- [41] Robin Rombach, Andreas Blattmann, Dominik Lorenz, Patrick Esser, and Björn Ommer. High-Resolution Image Synthesis with Latent Diffusion Models. In *2022 IEEE/CVF Conference on Computer Vision and Pattern Recognition (CVPR)*, pages 10674–10685, New Orleans, LA, USA, 2022. IEEE. 1
- [42] Chitwan Saharia, William Chan, Saurabh Saxena, Lala Li, Jay Whang, Emily L. Denton, Seyed Kamyar Seyed Ghasemipour, Raphael Gontijo Lopes, Burcu Karagol Ayan, Tim Salimans, Jonathan Ho, David J. Fleet, and Mohammad Norouzi. Photorealistic text-to-image diffusion models with deep language understanding. In *Advances in Neural Information Processing Systems 35: Annual Conference on Neural Information Processing Systems 2022, NeurIPS 2022, New Orleans, LA, USA, November 28 - December 9, 2022*, 2022. 1, 2
- [43] Axel Sauer, Frederic Boesel, Tim Dockhorn, Andreas Blattmann, Patrick Esser, and Robin Rombach. Fast high-resolution image synthesis with latent adversarial diffusion distillation. In *SIGGRAPH Asia 2024 Conference Papers, SA 2024, Tokyo, Japan, December 3-6, 2024*, pages 106:1–106:11. ACM, 2024. 2
- [44] Hengcan Shi, Munawar Hayat, Yicheng Wu, and Jianfei Cai. Proposalclip: Unsupervised open-category object proposal generation via exploiting CLIP cues. In *IEEE/CVF Conference on Computer Vision and Pattern Recognition, CVPR 2022, New Orleans, LA, USA, June 18-24, 2022*, pages 9601–9610. IEEE, 2022. 13
- [45] Haoyuan Sun, Bo Xia, Yongzhe Chang, and Xueqian Wang. Generalizing alignment paradigm of text-to-image generation with preferences through f-divergence minimization. In *AAAI-25, Sponsored by the Association for the Advancement of Artificial Intelligence, February 25 - March 4, 2025, Philadelphia, PA, USA*, pages 27644–27652. AAAI Press, 2025. 5
- [46] Aäron van den Oord, Yazhe Li, and Oriol Vinyals. Representation learning with contrastive predictive coding. *CoRR*, abs/1807.03748, 2018. 4
- [47] Timothy Alexis Vass. Explaining the SDXL latent space. <https://huggingface.co/blog/TimothyAlexisVass/explaining-the-sdxl-latent-space>, 2024. 5
- [48] Andrew Z. Wang, Songwei Ge, Tero Karras, Ming-Yu Liu, and Yogesh Balaji. A comprehensive study of decoder-only llms for text-to-image generation. In *IEEE/CVF Conference on Computer Vision and Pattern Recognition, CVPR 2025, Nashville, TN, USA, June 11-15, 2025*, pages 28575–28585. Computer Vision Foundation / IEEE, 2025. 5
- [49] Zhendong Wang, Jianmin Bao, Wengang Zhou, Weilun Wang, Hezhen Hu, Hong Chen, and Houqiang Li. DIRE for diffusion-generated image detection. In *IEEE/CVF International Conference on Computer Vision, ICCV 2023, Paris, France, October 1-6, 2023*, pages 22388–22398. IEEE, 2023. 3
- [50] Jinheng Xie, Weijia Mao, Zechen Bai, David Junhao Zhang, Weihao Wang, Kevin Qinghong Lin, Yuchao Gu, Zhijie Chen, Zhenheng Yang, and Mike Zheng Shou. Show-o: One single transformer to unify multimodal understanding and generation. In *The Thirteenth International Conference on Learning Representations, ICLR 2025, Singapore, April 24-28, 2025*. OpenReview.net, 2025. 2
- [51] Katherine Xu, Lingzhi Zhang, and Jianbo Shi. Good seed makes a good crop: Discovering secret seeds in text-to-image diffusion models. In *IEEE/CVF Winter Conference on Applications of Computer Vision, WACV 2025, Tucson, AZ, USA, February 26 - March 6, 2025*, pages 3024–3034. IEEE, 2025. 2
- [52] Qianqi Yan, Yue Fan, Hongquan Li, Shan Jiang, Yang Zhao, Xinze Guan, Ching-Chen Kuo, and Xin Eric Wang. Multimodal inconsistency reasoning (MMIR): A new benchmark for multimodal reasoning models. *CoRR*, abs/2502.16033, 2025. 13
- [53] Ling Yang, Zhilong Zhang, Yang Song, Shenda Hong, Runsheng Xu, Yue Zhao, Wentao Zhang, Bin Cui, and Ming-Hsuan Yang. Diffusion models: A comprehensive survey of methods and applications. *ACM computing surveys*, 56(4): 1–39, 2023. 2

- [54] Zhen Yang, Ganggui Ding, Wen Wang, Hao Chen, Bohan Zhuang, and Chunhua Shen. Object-aware inversion and re-assembly for image editing. In *The Twelfth International Conference on Learning Representations, ICLR 2024, Vienna, Austria, May 7-11, 2024*. OpenReview.net, 2024. [3](#)
- [55] Michal Yarom, Yonatan Bitton, Soravit Changpinyo, Roei Aharoni, Jonathan Herzig, Oran Lang, Eran Ofek, and Idan Szpektor. What you see is what you read? improving text-image alignment evaluation. In *Advances in Neural Information Processing Systems 36: Annual Conference on Neural Information Processing Systems 2023, NeurIPS 2023, New Orleans, LA, USA, December 10 - 16, 2023*, 2023. [5](#)
- [56] Xiaohua Zhai, Basil Mustafa, Alexander Kolesnikov, and Lucas Beyer. Sigmoid loss for language image pre-training. In *Proceedings of the IEEE/CVF international conference on computer vision*, pages 11975–11986, 2023. [2](#), [5](#)
- [57] Beichen Zhang, Pan Zhang, Xiaoyi Dong, Yuhang Zang, and Jiaqi Wang. Long-clip: Unlocking the long-text capability of CLIP. In *Computer Vision - ECCV 2024 - 18th European Conference, Milan, Italy, September 29-October 4, 2024, Proceedings, Part LI*, pages 310–325. Springer, 2024. [5](#)
- [58] Renrui Zhang, Chengzhuo Tong, Zhizheng Zhao, Ziyu Guo, Haoquan Zhang, Manyuan Zhang, Jiaming Liu, Peng Gao, and Hongsheng Li. Let’s verify and reinforce image generation step by step. In *IEEE/CVF Conference on Computer Vision and Pattern Recognition, CVPR 2025, Nashville, TN, USA, June 11-15, 2025*, pages 28662–28672. Computer Vision Foundation / IEEE, 2025. [2](#)
- [59] Youyuan Zhang, Jiuniu Wang, Hao Wu, and Wenjia Xu. Distinctive image captioning via CLIP guided group optimization. In *Computer Vision - ECCV 2022 Workshops - Tel Aviv, Israel, October 23-27, 2022, Proceedings, Part IV*, pages 223–238. Springer, 2022. [5](#)
- [60] Weihong Zhong, Xiaocheng Feng, Liang Zhao, Qiming Li, Lei Huang, Yuxuan Gu, Weitao Ma, Yuan Xu, and Bing Qin. Investigating and mitigating the multimodal hallucination snowballing in large vision-language models. In *Proceedings of the 62nd Annual Meeting of the Association for Computational Linguistics (Volume 1: Long Papers)*, pages 11991–12011, Bangkok, Thailand, 2024. Association for Computational Linguistics. [13](#)

## A. Non factual image-text pairs generation

In this section, we explain how we generate the necessary prompt corruptions for the Factual Consistency task, where encoders are employed to choose the most accurate prompt for a given image. Avoiding random LLM corruption, we define four specific dimensions of non-factuality to be corrupted (defined as `ERROR_TYPE` in the LLM prompt) [19, 52, 60].

The dimensions are as follows:

1. *Color*, which involves changing the color of the primary subject (e.g., an original caption with "a red apple" becomes "a green apple" in the corrupted version).
2. *Count*, which involves changing the number of the principal subject (e.g., if the original caption says "two dogs," the corrupted version changes it to "three dogs").
3. *Background*, which involves changing the setting of the main subject (e.g., a caption states "a cat on a mat" transforms to "a cat on a table" in the corrupted version).
4. *Main subject*, which involves changing the principal subject itself (e.g., original caption says "a bird on a branch," the corrupted version becomes "a squirrel on a branch").

To generate the misalignments, we use the instruction-tuned version of Gemma 3 with 27B parameters [21]. We employ this model to rewrite each original prompt based on the defined dimensions using the following prompt:

You are a highly specialized text transformation AI. Your sole task is to receive an original sentence and generate a single, corrupted version of that sentence.

Rules for Corruption:

1. **Maintain Original Structure:**  
The overall sentence flow must remain identical to the original.
2. **Targeted Non-Factuality:** Only modify the aspect of the sentence corresponding to the '`{ERROR_TYPE}`' provided. This modification should render that specific aspect non-factual or illogical within the context of the original sentence.
3. **Single Output:** Output only the corrupted sentence. No additional text, explanations, or formatting.
4. **Coherent Output:** Ensure that the output is coherent with the new

changes.

Change the `{ERROR_TYPE}` in the following PROMPT:

PROMPT: `{PROMPT}`

## B. Selecting the correct prompt

Furthering our analysis on Factual Consistency we now discuss how our method distinguishes different non-factual prompts and how that can influence the final results.

Analyzing recall@1 in Fig. 9, we compare how Noisy-CLIP selects the prompts along the generation. An overview shows that our model clearly distinguishes the accurate caption in the early latents. Despite the initial noise, our model reaches a recall@1 value greater than 0.5 in the middle of the generation.

As generation progresses, the selection of non-factual captions declines. The 'count' caption consistently maintains the highest recall among the non-factual options, this selection of a wrong captions is likely due to CLIP's known limitations in counting due its training on single-object images [25, 29, 44]. Considering the remaining non-factual captions from the middle of generation onward, the recall remains below 0.1, reinforcing the effectiveness of our approach when evaluating highly similar captions. Notably, the 'color' non-factual caption remains consistently below this threshold, while non-factual changes related to artifacts (subject or background) show similar selection behavior.

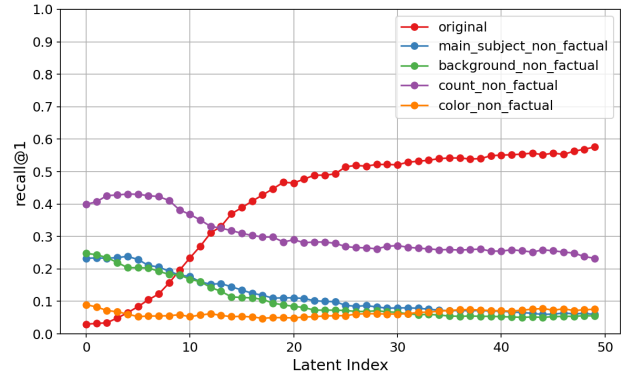


Figure 9. Examining Recall@1 in Caption Selection, we compare different prompt types, showing how different prompt corruptions affects the model's caption selection.

This analysis concludes that our approach's performance in ranking the non-factual alternatives is heavily influenced by input type. Specifically, we observed that "count" prompts yielded the highest recall, whereas "color" prompts showed the lowest, reinforcing known biases inherent to CLIP models.

Table 2. Quantitative comparison of fine-tuned encoders against baselines on GenAI-Bench [24], evaluated using VQAScore [26]. The table also reports Mean Value, giving the average score of all generated images.

Method	Basic						Advanced					Avg. Diff.	
	Attribute	Scene	Relation			Avg. Diff.	Count	Differ	Compare	Logical			Avg. Diff.
			Spatial	Action	Part					Negate	Universal		
<i>Denoised Latent (iteration 21-30)</i>													
NoisyCLIP	<b>0.831</b>	<b>0.854</b>	<b>0.817</b>	<b>0.821</b>	<b>0.820</b>	1.64	<b>0.738</b>	<b>0.709</b>	<b>0.721</b>	0.517	<b>0.676</b>	1.72	1.68
CLIP L14	0.819	0.853	0.805	0.808	0.799	2.82	0.716	0.688	0.683	<b>0.522</b>	0.674	3.28	3.05
<i>Final Image</i>													
CLIP L14	0.846	0.862	0.837	0.838	0.842	0	0.755	0.727	0.742	0.536	0.687	0	0
Mean Value	0.814	0.841	0.798	0.803	0.796	3.46	0.717	0.694	0.698	0.523	0.657	3.16	3.31

## C. Deeper analysis on Best-of-N Results

This analysis provides a more in depth analysis of twin-tower encoders selection in Noisy-GenAI-Bench using a best-of-10 evaluation approach. During this section, we assess the model’s capabilities across ten skill dimensions, splitted into basic and advanced prompts.

GenAI-Bench defines basic skills as core abilities such as, identifying visual attributes (e.g. color, material), contextual backgrounds, spatial relationships (e.g. an entity facing another), action dynamics (e.g. an entity pushing another), and part-whole configurations (e.g. a component is part of another, such as a body part). Simultaneously GenAI-Bench defines a set of advanced skills too, including counting, differentiation within categories (e.g. distinguish between two objects of the same category where one is "young" and another is "old", comparative characteristics (e.g. in a classroom there are more people standing than sitting), negation of attributes, and universal applicability (e.g. in a parking lot all cars are red).

This analysis compares the performance of NoisyCLIP and CLIP. We test their selection abilities during generation by choosing the best image between latents 21 and 30. Since CLIP was trained on non-noisy images, we also apply it to the final images. For this experiment, we report the VQAScore to show how well the selected images align with the prompts.

### C.1. Basic Prompts

Table 2 shows that the fine-tuned approaches consistently outperformed both the frozen baseline and the mean value of all skills. Selecting a random image would achieve a result that lacks 3.46% to the final clip selection. While CLIP in the middle of the generation has a difference of 2.82% to the final selection, our model NoisyCLIP can achieve the best results putting that difference down to 1.64%.

Looking more into depth in the Attribute skill, when using CLIP to select an image during the generation, lacks by

2.7% while our approach bring that down to 1.5%, showing that our model is capable of select images that better depict attributes of entities such as colors and materials. On the other hand when we go to generations that obligate to focus more on the overall scene such as backgrounds and settings the results are pretty similar between our approach and CLIP achieving both a great result of being 0.8% below the score of using CLIP to select the image after being generated.

The spatial relationship results revealed even more interesting findings, as CLIP in the mid-generation phase scores 3.2% lower than in the final images. Our method improves alignment by 1.2%, showcasing its ability to capture physical relations between multiple entities, such as "a cat on the right and a dog on the left". This indicates that our model not only detects entities in noisy conditions, but also captures the differences between them, selecting an image that can achieve closer results to the final CLIP score. Action and Part splits take a similar approach where our model can improve performance of the CLIP in the middle of the generation by up to 2.1%.

### C.2. Advanced Prompts

The results presented in Table 2 demonstrate the effectiveness of our method with "advanced" prompts, highlighting its robust ability to select images that closely match more complex textual descriptions. The lower average score for these images accurately reflects the inherent challenge that generative models and twin-tower encoders face when interpreting complex prompts compared to simpler, basic prompts. However, our method improves by 1.56% in the latent space and by 1.44% in mean value over the frozen model. Interestingly, as prompt difficulty increases, using a randomly selected image can sometimes align better than employing the frozen CLIP midway through generation, evidenced by an average difference of 3.16% compared to 3.28%.



Table 3. Alignment assessed across both GenAI-Bench splits. The table presents the alignment scores for each model, and for the denoised latent output, the alignment is also shown as a percentage of the final image score, offering a thorough perspective on alignment performance.

Method	Alignment	
	Basic	Advanced
<i>Denoised Latent (iteration 21-30)</i>		
NoisyCLIP	<b>0.262 (88.5%)</b>	<b>0.250 (90.6%)</b>
CLIP L14	0.183 (19.8%)	0.186 (67.4%)
<i>Final Image</i>		
CLIP L14	0.296	0.276

Looking at the performance per skill, NoisyCLIP shows a 2.2% improvement in selection accuracy for prompts that specify quantity or size. This suggests that our approach helps mitigate the known limitations of CLIP regarding counting, particularly under noisy conditions. For captions requiring differentiation (e.g., "one cat is sleeping on the table and the other is playing under the table"), we observed a further 2.1% improvement. This demonstrates that our model can significantly enhance the overall image alignment even with complex spatial or relational descriptions, all while reducing the necessary diffusion steps.

In the comparison skill, our model achieves a 3.8% improvement over CLIP selection during the generation process, indicating a clear advantage. Consistent with the baseline, our approach struggles most with negation prompts, such as those where entities are missing or actions are unexecuted (e.g., "a shelf without books"). This challenge is common due to the limited negation examples in training datasets, as noted by [31], with no reported method exceeding a score of 54%. Similarly, all approaches struggle with universal attribute sharing, with no method exceeding 70%.

These results, despite the increased prompt complexity, validate our initial findings: our method remains superior in assessing alignment and selecting the optimal image within the latent space, successfully overcoming challenges from noisy intermediate representations. However, it is important to note that our results also show that known limitations of CLIP, particularly its difficulty with negation, transfer directly to the noisy latent space results too.

## D. Alignment

In this experiment, we examine the variations in alignment scores produced by NoisyCLIP and CLIP during the mid-generation phase and compare these results to the score of CLIP on the final output, across both splits of the Noisy-GenAI-Bench.

Specifically, with basic prompts, NoisyCLIP reaches

Table 4. Comparative analysis of performance improvements when training only the image encoder compared to joint training with the text encoder.

Model	GenAI	
	Basic	Advanced
<i>Denoised Latent (iteration 21-30)</i>		
Frozen	0.821	0.633
+ Image Encoder	<b>0.836</b>	<b>0.646</b>
+ Text Encoder	0.835	0.645
<i>Image Dimension</i>		
Frozen	0.856	0.664
+ Image Encoder	<b>0.858</b>	<b>0.664</b>
+ Text Encoder	0.856	0.657

88.5% of the final score during the mid-generation stage, significantly outperforming the CLIP baseline, which only achieves 19.8%. In contrast, when using advanced prompts, NoisyCLIP achieves 90.6% of the final score, while CLIP baseline achieves 67.4%. Our approach shows a major gain over the baseline, indicating that fine-tuning on noisy latent data can substantially improve similarity measurement in the middle of the generation, achieving over 90% of the final score.

## E. Ablation Studies

### E.1. Impact of Trained Encoders

To evaluate how the trained modalities influence the performance of NoisyCLIP, we report experiments that evaluate three approaches: a frozen baseline, training the image encoder, and a fully trained text and image encoder on the Noisy-GenAI-Bench. As illustrated in Table 4, both training approaches show enhancements in both subsets. In particular, training only the image encoder consistently delivers the best results. Within the latent dimension, the differences between the image-trained model and the fully trained model are relatively small, while the difference compared to the frozen baseline is more significant (up to 1.3%). However, in the image dimension, the text encoder demonstrated a worse performance than the frozen baseline, particularly within the 'Advanced' subset, while the trained image encoder maintained comparable or superior results.

The study shows that training the image encoder is critical for performance, offering up to 1.5% gains over the baseline, confirming our choice to prioritize image encoder optimization to increase the capabilities of the twin-tower encoder under noise.

## E.2. Analysis on Scaling Model Size

To evaluate the correlation between model size and performance, we compared NoisyCLIP using two different encoder sizes, ViT-B/16 (150M parameters) and ViT-L/14. These results are presented in Table 5, focusing on performance in the Basic and Advanced subsets of NoisyGenAI-Bench. The results consistently show a positive correlation between model size and performance when fine-tuned. The larger ViT-L/14 encoder generally surpasses the smaller ViT-B/16 across both evaluation settings. In the latent dimension, ViT-L/14 outperformed ViT-B/16 by 0.7% on the Basic set and 0.5% on the Advanced set. The advantage was more pronounced in the Image Dimension setting, where ViT-L/14 scored 0.858 and 0.664, surpassing ViT-B/16 scores (0.854 and 0.652) by 0.5% and 1.8%, respectively. This ablation study validates that scaling the encoder size is an effective strategy to improve performance even in this noisy environment, suggesting that models with higher parameter counts possess a greater capacity to learn robust representations. With this we cannot discard the fact that the relatively small difference in final scores indicates that even the smaller ViT-B/16 encoder achieves very competitive results.

Table 5. Analysis of performance improvements by varying the encoder size (Evaluated at Latent Dimension Steps 21-30)

Encoder	Encoder Size	GenAI Score	
Size	(Parameters)	Basic	Advanced
Denoised Latent (iteration 21-30)			
ViT-B/16	150M	0.829	0.643
ViT-L/14	428M	<b>0.836</b>	<b>0.646</b>
Image Dimension			
ViT-B/16	150M	0.854	0.652
ViT-L/14	428M	<b>0.858</b>	<b>0.664</b>

## F. Further Analysis of Qualitative Results

### F.1. Analysis of Edge Scenarios on Best-of-N

This section extends the qualitative results by presenting an analysis of borderline cases and edge scenarios in the task of image selection during and after the generation process.

In Figure 10 (top), the first example demonstrates NoisyCLIP’s ability to select an image with alignment equal to or better than post-generation CLIP, whereas CLIP applied during generation lacks overall compositional quality. The second example, despite the poor generated images, shows NoisyCLIP selecting the closest match to the prompt; while the generation CLIP incorrectly reverses the order of the utensils, NoisyCLIP chooses the image most representative

of the text. The third prompt highlights NoisyCLIP’s efficiency, selecting an image comparable to the final CLIP while significantly reducing the required diffusion steps.

However, the fourth example shows a failure case for NoisyCLIP where it selects what appears to be a hallucination. This likely occurred because the generation model failed to produce the requested object and instead focused on an unintended entity (the genie), which NoisyCLIP mistakenly prioritized. The fifth and final prompts show scenarios where all methods result in divergent selections and none perfectly match the prompt. In the fifth case, different methods focus on either a ball or a frisbee, as no generated image depicts both. Similarly, the final prompt leads all methods to select different, yet imperfect, images.

In the second row of examples (Figure 10 (bottom)), the second example again depicts a scenario where no image was correctly generated, resulting in all methods failing to select an accurate representation of the prompt. The third prompt highlights a limitation of our approach, where it over-focuses on the initial part of the prompt while omitting the important "frosty glass of water".

The fourth and fifth prompts illustrate cases where all models exhibit hallucinations regarding the count of entities. Specifically, in the fifth prompt, CLIP (in both configurations) selects an image featuring the three required animals (two birds instead of one) but incorrectly includes two chairs instead of the one specified. In contrast, our approach selects an image that correctly depicts a single chair as prompted, but entirely misses the dog and contains incorrect counts of other entities. This strong divergence suggests that with complex, multi-entity prompts, selection choices can highly vary based on the prioritization of different attributes.

The sixth prompt shows a case where the weaker method (CLIP selection during generation) still yielded the best-aligned image. This highlights that post-generation selection can also wrongly select hallucinations and that NoisyCLIP is susceptible to misunderstanding and the swapping of elements’ attributes.

### F.2. Examples of Middle Diffusion Scoring

To conclude we present results illustrating the behaviour of the scoring functions during the reverse diffusion process (Figure 11). Each example shows a prompt and three generation stages, an early noisy latent (step 10), a middle-point latent (step 25), and the final image. We measured prompt-image similarity using both NoisyCLIP and CLIP in each depicted stage. Overall, our model consistently achieves scores in the middle of the generation that closely correlate with the final scores. This demonstrates how our approach enables twin-tower encoders to effectively measure similarity under noisy conditions, allowing for an accurate assessment of the prompt-to-image alignment mid-generation.











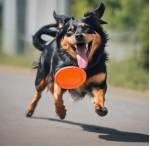













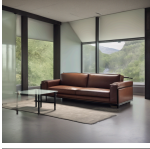
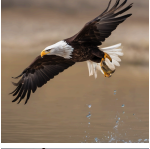



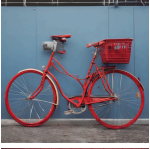






	A flat screen mounted above a rectangular fireplace	On the left is a wooden spoon and on the right is a metal fork.	A band of beetles playing rock music on miniature instruments, with a leaf as stage.	A genie's lamp emitting wisps of smoke on a sandy dune.	A cheerful dog with a frisbee in its mouth on the right, chasing a rolling ball on the left.	A cup set to the right of a newspaper.	Image Selection Criteria
CLIP							after generation
CLIP							during genatation
NoisyCLIP							during generation
	A leather couch positioned invitingly in front of a large, glass television screen.	An eagle soaring with a fish in its talons.	A table coaster with an intricate mosaic design under a frosty glass of water	A dog, a cat and a chicken on a table.	A dog, a cat and a bird on a chair.	A red bicycle against a blue wall.	Image Selection Criteria
CLIP							after generation
CLIP							during genatation
NoisyCLIP							during generation

Figure 10. Images are generated using a best-of-6 strategy. Our proposed method is compared against the standard CLIP baseline at two computation budgets: a fixed lower cost and the full cost (generating all 6 images).



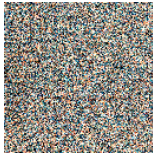






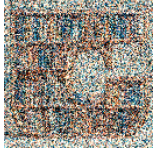

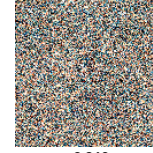
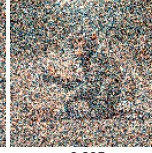


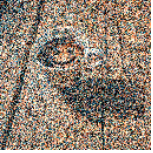



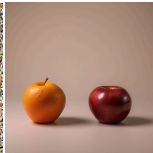
Prompt	10	25	Final Image	Prompt	10	25	Final Image
A modern bench with clear acrylic top and wooden floor, set against a gray wainscoted wall.				A white coffee cup with a heart-shaped milk foam design sits on a wooden table next to an Apple laptop.			
	NoisyCLIP 0.222	0.330	0.322		NoisyCLIP 0.143	0.262	0.332
	CLIP 0.065	0.137	0.348		CLIP 0.055	0.084	0.281
A woman in a black dress and a man in a beige suit smile at the camera, both appearing to be at a formal event.				A monkey sits on a road, holding food, with a pinkish face and gray body, surrounded by other monkeys in the background.			
	NoisyCLIP 0.195	0.338	0.396		NoisyCLIP 0.248	0.285	0.354
	CLIP 0.131	0.178	0.383		CLIP 0.153	0.239	0.359
A white mug filled with dark liquid, resembling a smiling face, sits on a wooden surface with a warm, natural wood grain pattern.				Two fruits, an apple and an orange, sit side by side on a plain background, highlighting their distinct features.			
	NoisyCLIP 0.162	0.195	0.350		NoisyCLIP 0.195	0.303	0.299
	CLIP 0.091	0.133	0.379		CLIP 0.111	0.245	0.290

Figure 11. Image generation process using NoisyCLIP and CLIP for early alignment assessment during generation.